Separation and Purification Technology 331 (2024) 125559

Contents lists available at ScienceDirect

Separation and Purification Technology

journal homepage: www.elsevier.com/locate/seppur

Adsorption modeling for contaminant removal in plastic dissolution recycling: Investigating an amino ketone-based red dye

Michiel Van Melkebeke [a], Tobias De Somer [a], Tine Van Laere [a], Thien Nguyen Luu Minh [a], Hamed Mohamadzadeh Shirazi [b], Hilde Poelman [b], Kevin Van Geem [b], Steven De Meester [a,*]

[a] Laboratory for Circular Process Engineering (LCPE), Department of Green Chemistry and Technology, Ghent University, Graaf Karel de Goedelaan 5, Kortrijk 8500, Belgium

[b] Laboratory for Chemical Technology (LCT), Department of Materials, Textiles and Chemical Engineering, Ghent University, Technologiepark Zwijnaarde 125, Zwijnaarde B-9052, Belgium

ARTICLE INFO

Keywords:
Plastic recycling
Adsorption
Dye removal
Solvent
Statistical physics modeling

ABSTRACT

The widespread inclusion of additives in plastics has posed a significant challenge to increasing global plastic recycling rates. This study explores the potential of adsorption in non-aqueous environment as a novel approach for plastic waste dissolution recycling. Activated charcoal was selected as the adsorbent for the removal of Solvent Red 135, a commonly used amino ketone-based dye, from polystyrene (PS) solutions. Three solvents, namely o-xylene, limonene, and butyl acetate, were investigated. Adsorption experiments were conducted at 293 K, and the results were analyzed using both classical and statistical physics models. The activated charcoal exhibited the highest single component adsorption capacity for the dye when butyl acetate was used as the solvent, while it showed negligible adsorption for PS in all three solvents. When dealing with mixtures of the dye and 1.0 wt% PS in butyl acetate, a removal efficiency of 99% was achieved at an adsorbent dose of 2.0 g L^{-1}. However, when the PS concentration in the solvent increased to 10 wt%, the required adsorbent dose rose to 3.3 g L^{-1}. Modeling results indicated that monolayer adsorption occurred via a multi-molecular adsorption mechanism, with an approximate adsorbed dye molecule count of 1.5 per adsorption site. The adsorption energy for all three solvents ranged between 0 and 40 kJ mol^{-1}, indicating that the adsorption process is predominantly driven by physical forces and is an endothermic process. This study presents a foundational assessment of adsorption as an effective solvent-based technique for the removal of additives in plastic recycling.

1. Introduction

Plastics have transformed our society by allowing cheap, lightweight and functional applications in packaging, construction, textiles, consumer products, transportation, electronics, healthcare and many more [1–4]. This currently mounts up to a global plastic production of approximately 380 million tons per year. Owing to their increasing functionality and decreasing production cost, this number is expected to rise over the next few decades [5]. The latter inevitably translates to a growing amount of plastic waste, which without proper management causes harm to the environment [6]. Today, 40% of plastic waste is still being landfilled and merely 14% is collected for recycling [7]. Although recycling rates vary among countries, with approximately 10% for the US and 31% for Europe, it is evident that the plastic production and recycling industry are facing a considerable challenge [2,8].

Traditional mechanical recycling is unable to remove persistent contaminants (e.g. non-polar VOC's) and plastic additives (e.g. colorants), while also suffering from thermal–mechanical degradation and immiscibility of different polymer types. This ultimately leads to the production of lower value applications, a process known as downcycling [9,10]. Chemical recycling, which involves breaking of the polymer chains, is able to process plastic waste that is difficult to treat mechanically (e.g. multilayer packaging), yet also suffers from the presence of impurities and additives, leading to operational issues such as coking, catalyst poisoning and corrosion [10–13]. Thus, encouraged by ambitious policies such as the Circular Economy Package imposed by the European Commission [14], additive extraction technologies are gaining interest [15]. Among these technologies, solid–liquid extraction and dissolution-precipitation are the most prominent [16]. Due to the critical impact of colorants on the quality of the recycled product, much

* Corresponding author.
E-mail address: steven.demeester@ugent.be (S. De Meester).

https://doi.org/10.1016/j.seppur.2023.125559
Received 8 July 2023; Received in revised form 27 October 2023; Accepted 30 October 2023
Available online 7 November 2023

attention has been given to the removal of this type of additive [17]. An important classification of colorants is based on their physical behavior, distinguishing dyes from pigments. Dyes are organic substances that are soluble in the polymer matrix, while pigments can be organic or inorganic substances that are insoluble in the polymer matrix [18,19].

Considering solid–liquid extraction methods, the removal of undissolved contaminants is hampered as the migration of such suspended particles of considerable (molecular) size in the polymer matrix is very limited in its solid state [16,20]. And while there are some dissolution-precipitation processes available on the market [21–24], there is little scientific knowledge on the behavior of additives, including dyes and pigments, in this process [16]. Creating more understanding of this is crucial as dyes and other dissolved substances are removed based on their solubility differences with the polymer in the solvent–antisolvent mixture [16,25]. Typically, dissolution recycling proposes filtration as a technique to remove (undissolved) contaminants, yet, in case of dissolved contaminants (e.g. non-polar organic substances which include many additives) these would migrate through the filter together with the polymer and the solvent.

To avoid these drawbacks, the present paper proposes adsorption during the dissolution recycling of plastics, as a first to the best of our knowledge. Adsorption is a separation technique that is widely used for water treatment among others due to its low energetic requirements and simple implementation and operation in comparison with other unit operations [26–32]. There is, however, little literature available on adsorption applications in non-aqueous or non-polar environments. A number of studies suggest adsorption as a purifying technique for different types of oil, mainly involving the removal of oxygen, nitrogen, sulfur and chlorinated compounds from crude and pyrolysis oils [33–37]. Fundamental research into the removal of plastic additives by means of adsorption in organic solvents is largely lacking. The main objective of this work is thus to provide a first evaluation of adsorption as an additive extraction technique by studying the adsorption behavior of a prevalent plastic additive in different polymer solutions.

Screening of different types of commercially available (typical) adsorbents, including silica, alumina, molecular sieves, carbonaceous and polymeric materials, revealed that the performance of activated charcoal was superior (Table S1). In addition, activated carbons score generally excellent in terms of regeneration, which can be done thermally, chemically, electrochemically, biologically, or via microwave irradiation, among others [38–43]. Using the latter adsorbent type, a comprehensive study on the adsorption mechanism of the dye Solvent Red 135 was conducted in polystyrene (PS) solutions. Solvent Red 135 is a food-contact approved amino ketone-based dye that is applicable to a wide range of polymers, including PS, polycarbonate (PC), polyethylene terephthalate (PET), polyvinyl chloride (PVC) and acrylonitrile butadiene styrene (ABS) [44]. Then again, polystyrene is one of the most popular plastics, widely used in the packaging industry and hence making up a substantial fraction of the total plastic waste generated [2,45]. For the dissolution recycling of PS, three different organic solvents were used, being o-xylene, butyl acetate and limonene. Butyl acetate is a type of ester that has a higher polarity than o-xylene, which is a traditional aromatic solvent. Limonene is an aliphatic hydrocarbon classified as a cyclic monoterpene, which is produced from renewable sources and therefore considered as a green solvent [46]. The present work modeled both kinetics and adsorption isotherms to fit the experimental data. Aside from the many classical isotherm models that have been proposed, such as the Langmuir and Freundlich models, this study also includes the statistical physics approach, where the parameters reflect the state of the adsorption system rather than being part of a merely empirical expression. This allows for a thorough analysis of the adsorption phenomena at a molecular scale [47].

2. Materials and methods

2.1. Materials

The activated charcoal powder was purchased from Merck KGaA. Solvent Red 135 was supplied by Sun Chemical Colors & Effects GmbH in a pure powder form under the product name Oracet™Red 344. Its molecular structure is presented in Figure S1. General purpose PS in the form of Styron™ 634 pellets was acquired from Resinex. The solvents o-xylene with a purity of 99%, n-butyl acetate with a purity of 99% and (*R*)-limonene with a purity of 96% were procured from Fisher Scientific Inc.

2.2. Characterization of adsorbent

The nitrogen adsorption–desorption isotherm was used to characterize the activated charcoal by means of a Micromeritics Tristar II 3020 Analyzer operating at 77 K. A Brunauer–Emmett–Teller (BET) analysis was performed to calculate the specific surface area (S_{BET}) [48]. The t-plot method was used to determine the external surface area (S_{ext}), the micropore area (S_{micro}) and the total micropore volume (V_{micro}) [49]. The total pore volume (V_{tot}) and the average pore width (W_{avg}) were estimated using the Barrett–Joyner–Halenda (BJH) [50]. Fourier transformed infrared spectroscopy (FTIR) using a Nicolet™ iS20 FTIR Spectrometer was used to identify changes in surface chemistry before and after adsorption. To examine the morphological features of the adsorbent before and after adsorption, scanning electron microscopy (SEM) was applied using a JEOL JSM-7600F.

2.3. Preparation and calibration

For the preparation of the adsorbent, the activated charcoal powder was dried in an oven at 80 °C for 12 h. Afterwards, the material was cooled down to room temperature in a desiccator to avoid contamination with water vapor present in air, among others. To obtain calibration curves of absorbance versus adsorbate concentration, the maximum absorption wavelengths of the dye and polymer in the three organic solvents were determined by means of a Biochrom WPA Lightwave II UV–Vis spectrophotometer. From this, the calibration curves were determined up to a maximum concentration of 60 mg L^{-1} and 60 g L^{-1} for the dye and polymer, respectively (Fig. S2).

2.4. Adsorption isotherm experiments

In a first scenario, the adsorption isotherm experiments of the dye and polymer were independently conducted in the three organic solvents at 293 ± 1 K. Initial concentrations were varied from 1 to 50 mg L^{-1} and from 1 to 50 g L^{-1} for Solvent Red 135 and PS, respectively. In a second scenario, solutions of 1.0 wt% PS were prepared with varying dye concentrations from 1 to 50 mg L^{-1}. For both scenarios, solutions of 100 mL were mixed with a fixed adsorbent mass of 10 mg and subsequently stirred at 300 rpm for at least 12 h to reach an equilibrium state. The latter was considered to be attained when the adsorbate concentration in the liquid phase remained constant for three consecutive measurements (i.e. standard deviation lower than 5 %) [30]. Samples were centrifuged at 4000 rpm and the supernatant was analyzed via the UV–Vis spectrophotometer to determine the equilibrium concentration of the adsorbate. Experiments were triplicated for all examined adsorbate concentrations (i.e. Solvent Red 135 solutions, PS solutions, and mixtures). The amount of adsorbate adsorbed at equilibrium was calculated as follows:

$$q_e = \frac{(C_0 - C_e)\,V}{m} \tag{1}$$

where q_e is the amount of adsorbate adsorbed at equilibrium (mg g^{-1}), C_0 is the initial adsorbate concentration (mg L^{-1}), C_e is the adsorbate concentration at equilibrium (mg L^{-1}), m is the adsorbent mass (g) and V the solution volume (L).

2.5. Adsorption kinetic experiments

Adsorption kinetics of the dye (with PS) were studied in the three organic solvents at 293 ± 1 K. Solutions of pure PS were not considered due to the negligible adsorption capacity derived from preceding adsorption experiments. Initial dye concentrations were set to 40 mg L^{-1}. In a first stage, no PS was added. In a second stage, the solutions were adjusted to hold 1.0 wt% PS. Solutions of 100 mL were analogously mixed with an adsorbent mass of 10 mg and stirred at 300 rpm. The adsorption time was varied until equilibrium was obtained. Again, experiments were triplicated for each solvent. The amount of adsorbate adsorbed after a certain period of time was calculated as follows:

$$q_t = \frac{(C_0 - C_t)\,V}{m} \tag{2}$$

where q_t is the amount of adsorbate adsorbed at time t (mg g^{-1}), C_0 is the initial adsorbate concentration (mg L^{-1}), C_t is the adsorbate concentration at time t (mg L^{-1}), m is the adsorbent mass (g) and V the solution volume (L).

2.6. Removal efficiency study

Adsorption experiments were performed with increasing adsorbent dose to evaluate the effect on the removal efficiency of the plastic dye. The adsorbent dose was varied from 0.1 to 10 g L^{-1}. In a first case, Solvent Red 135 solutions were prepared without the addition of PS. The initial dye concentration was set to 40 mg L^{-1} for all three solvents. In a second case, the red dye was dissolved in 1.0 wt% PS solutions. The Solvent Red 135 concentration was again 40 mg L^{-1}, ensuring a realistic concentration of the dye in the polymer matrix of approximately 0.5 wt% [19,51]. In a third and final case, the PS concentration was increased to 10.0 wt%, allowing evaluation in terms of practical feasibility. For comparison reasons, the concentration of the dye was maintained at 40 mg L^{-1}. The experiments were triplicated and conducted on all three solvents. The removal efficiency was calculated as follows:

$$R = \left(\frac{C_0 - C_e}{C_0}\right) \times 100 \tag{3}$$

where R is the removal efficiency (%).

In addition, the adsorption capacity of the adsorbent for the dye was regenerated for the best performing solvent in order to investigate the reusability. To that end, an adsorbent dose of 0.5 g L^{-1} was selected for a 100 mL solution with a Solvent Red 135 concentration of 40 mg L^{-1}. Similar to earlier work, the treated adsorbent was regenerated via desorption through consecutively exposing it to pure solvent until the concentration of the dye in the medium was negligible [52,53]. The adsorbent material was dried in an oven at 80 °C for 4 h. Ultimately, the removal efficiency was determined in triplicate for a total of three regeneration cycles.

2.7. Modeling analysis

2.7.1. Adsorption isotherms

Adsorption isotherms give the relation between the amount of adsorbate adsorbed in the solid phase (by the adsorbent) and the amount of adsorbate remaining in the liquid phase, when the two phases are in dynamic equilibrium at a specified temperature. From these equilibrium curves, important information about the adsorption system can be derived, such as the maximum adsorption capacity and the interaction mechanism between adsorbent and adsorbate. Therefore, a vast number of equations have been developed to describe adsorption phenomena.

The isotherm model proposed by Langmuir is the most conventional to describe monolayer adsorption and is given by [54]:

$$q_e = \frac{q_{mL} k_L C_e}{1 + k_L C_e} \tag{4}$$

where q_{mL} is the Langmuir maximum adsorption capacity (mg g^{-1}) and k_L the Langmuir constant (L mg^{-1}). The simplicity of this model is based on four assumptions [55]: (1) only monolayer coverage can occur, (2) adsorption sites can hold only one adsorbate molecule, (3) adsorption sites are energetically equivalent and their distribution is homogeneous, and (4) the ability of an adsorbate molecule to adsorb on a given adsorption site is independent of the occupation of a neighboring adsorption site.

Important adjustments to these assumptions have been considered by other isotherm models. The equation suggested by Freundlich is a widely adopted one [56]:

$$q_e = k_F C_e^{\frac{1}{n_F}} \tag{5}$$

where k_F is the Freundlich constant (L mg^{-1}) and $\frac{1}{n_F}$ is the heterogeneity factor. This model assumes that adsorption occurs on a heterogeneous surface with non-identical adsorption sites and attempts to account for the interactions between adsorbate molecules.

Another isotherm model is proposed by Temkin, who states that the adsorption process is characterized by a uniform distribution of the binding energies up to some maximum value. The heat of adsorption is said to decrease linearly with coverage as a result of the interactions between adsorbent and adsorbate molecules. The Temkin model is given by [57]:

$$q_e = \frac{RT}{b_T}\, ln(k_T C_e) \tag{6}$$

where R is the universal gas constant (8.31 J mol^{-1} K^{-1}), T is the absolute adsorption temperature (K), b_T is the Temkin constant related to adsorption heat (J mol^{-1}) and k_T is the Temkin equilibrium constant (L mg^{-1}).

The Dubinin–Radushkevich (D–R) isotherm model argues that the dynamic adsorption equilibrium can be expressed independently of temperature by utilizing the adsorption potential [58]:

$$\varepsilon = RT\, ln\left(1 + \frac{1}{C_e}\right) \tag{7}$$

where ε is the adsorption potential (kJ mol^{-1}) based on Polanyi's potential theory. The D-R model is subsequently given by:

$$q_e = q_{mD}\, e^{-\beta\varepsilon^2} \tag{8}$$

where q_{mD} is the D-R maximum adsorption capacity (mg g^{-1}) and β is a measure of the sorption free energy (mol^2 kJ^{-2}).

A three parameter model was proposed by Redlich and Peterson (R–P) to describe the adsorption process over a wide range of concentrations for both homogeneous and heterogeneous systems. It is considered a hybrid model of the Langmuir and Freundlich expressions [59]:

$$q_e = \frac{k_R C_e}{1 + a_R C_e^{b_R}} \tag{9}$$

where k_R (L g^{-1}) and a_R (L mg^{-1}) are the R-P model constants and b_R is the R-P model exponent, which may vary between 0 and 1. Next to the R-P model, there exist many other empirical equations with three or four parameters such as the Sips and the Fritz–Schlunder isotherm models [60,61]. They are, however, mostly simple modifications of the Langmuir and Freundlich models, with minimal additional significance in adsorption studies. Therefore, they will not be considered in this work.

For the case where the formation of multilayers is expected, the most widely used equation is the BET isotherm, initially developed by Brunauer et al. for solid–gas systems and later reformulated for solid–liquid systems by Ebadi et al. [48,62]:

$$q_e = \frac{q_B k_{B1} C_e \left[1 - (n_B + 1)\,(k_{B2} C_e)^{n_B} + n_B\,(k_{B2} C_e)^{n_B+1}\right]}{(1 - k_{B2} C_e)\left[1 + \left(\frac{k_{B1}}{k_{B2}} - 1\right) k_{B2} C_e - \left(\frac{k_{B1}}{k_{B2}}\right)(k_{B2} C_e)^{n_B+1}\right]} \tag{10}$$

where q_B is the monolayer adsorption capacity (mg g^{-1}), k_{B1} (L mg^{-1}) and k_{B2} (L mg^{-1}) are the BET model constants for the first and outer layer, respectively, and n_B is the total number of adsorption layers.

Aside from the previous empirical models that are traditionally used, this work also includes three statistical physics models. These models are more complex, but are of added value because they offer more meaningful interpretations [47,63–70]. The first expression represents a monolayer model in which the adsorbed molecules form a single layer with one energy of adsorption:

$$q_e = \frac{nN_M}{1 + \left(\frac{C_{1/2}}{C_e}\right)^n} \tag{11}$$

where n is the number or fraction of molecules per adsorption site, N_M is the density of identical adsorption sites occupied by adsorbate molecules (mg g^{-1}) and $C_{1/2}$ is the adsorbate concentration at half-saturation (mg L^{-1}). Note that when n equals 1, the model simplifies to the Langmuir isotherm.

The second expression considers a double layer model where adsorption can take place onto two different layers with two separate adsorption energies:

$$q_e = nN_M \frac{\left(\frac{C_e}{C_1}\right)^n + 2\left(\frac{C_e}{C_2}\right)^{2n}}{1 + \left(\frac{C_e}{C_1}\right)^n + \left(\frac{C_e}{C_2}\right)^{2n}} \tag{12}$$

where C_1 (mg L^{-1}) and C_2 (mg L^{-1}) are the adsorbate concentrations at half saturation associated with the first and second layer, respectively.

The third expression assumes that the adsorption process results in the formation of an adjustable, yet restricted number of layers with two adsorption energies:

$$q_e = nN_M \frac{F_1(C) + F_2(C) + F_3(C) + F_4(C)}{G(C)} \tag{13}$$

$$F_1(C) = -\frac{2\left(\frac{C_e}{C_1}\right)^{2n}}{1 - \left(\frac{C_e}{C_1}\right)^n} + \frac{\left(\frac{C_e}{C_1}\right)^n \left(1 - \left(\frac{C_e}{C_1}\right)^{2n}\right)}{\left(1 - \left(\frac{C_e}{C_1}\right)^n\right)^2} \tag{14}$$

$$F_2(C) = \frac{2\left(\frac{C_e}{C_1}\right)^n \left(\frac{C_e}{C_2}\right)^n \left(1 - \left(\frac{C_e}{C_2}\right)^{nN_2}\right)}{1 - \left(\frac{C_e}{C_2}\right)^n} \tag{15}$$

$$F_3(C) = -N_2 \frac{\left(\frac{C_e}{C_1}\right)^n \left(\frac{C_e}{C_2}\right)^n \left(\frac{C_e}{C_2}\right)^{nN_2}}{1 - \left(\frac{C_e}{C_2}\right)^n} \tag{16}$$

$$F_4(C) = \frac{\left(\frac{C_e}{C_1}\right)^n \left(\frac{C_e}{C_2}\right)^{2n} \left(1 - \left(\frac{C_e}{C_2}\right)^{nN_2}\right)}{\left(1 - \left(\frac{C_e}{C_2}\right)^n\right)^2} \tag{17}$$

$$G(C) = \frac{\left(1 - \left(\frac{C_e}{C_1}\right)^{2n}\right)}{1 - \left(\frac{C_e}{C_1}\right)^n} + \frac{\left(\frac{C_e}{C_1}\right)^n \left(\frac{C_e}{C_2}\right)^n \left(1 - \left(\frac{C_e}{C_2}\right)^{nN_2}\right)}{\left(1 - \left(\frac{C_e}{C_2}\right)^n\right)^2} \tag{18}$$

where C_1 and C_2 are now the adsorbate concentrations at half saturation associated to the first and the $N_2 + 1$ layers, respectively. The parameter N_2 reflects the formed layers where the total number of layers is $N_2 + 1$. Note that when N_2 equals 0 and n equals 1, the model again simplifies to the Langmuir isotherm.

2.7.2. Adsorption kinetics

Adsorption kinetics express the rate of adsorbate removal from the fluid phase to the solid phase. It provides insight into the required residence time to obtain the desired adsorbate concentration, which is essential for the design and operation of adsorption equipment. Several mathematical models have been suggested to describe the kinetics of adsorption processes. The pseudo-first-order and pseudo-second-order are the most extensively used in adsorption studies. Next to these models, the present work also includes the Elovich model to investigate potential chemisorption, and the Weber–Morris model to evaluate the intraparticle diffusion process as the only rate controlling step [30,71–73].

The pseudo-first-order expression is an adsorption reaction model, describing the adsorption process as a single phenomenon and is presented by Lagergren as [74]:

$$\frac{dq_t}{dt} = k_1 \left(q_e - q_t\right) \tag{19}$$

where k_1 is the pseudo-first-order rate constant (min^{-1}).

The pseudo-second-order expression can also be classified as an adsorption reaction model and was first described by Ho et al. as follows [75]:

$$\frac{dq_t}{dt} = k_2 \left(q_e - q_t\right)^2 \tag{20}$$

where k_2 is the pseudo-second-order rate constant (g mg^{-1} min^{-1}).

The Elovich expression is used to describe the kinetics of chemisorption processes, initially of gaseous adsorbate molecules, but more recently also of solid–liquid systems [72]. The model is defined as [76]:

$$\frac{dq_t}{dt} = a_E e^{-b_E q_t} \tag{21}$$

where a_E is the initial adsorption rate constant (mg g^{-1} min^{-1}) and b_E is the desorption rate constant (g mg^{-1}).

The Weber–Morris expression is a conventional intraparticle diffusion model that assumes that the diffusion of adsorbate molecules within the adsorbent pores is the rate controlling step. It is presented as follows [77]:

$$q_t = k_W \sqrt{t} + W \tag{22}$$

where k_W is the intraparticle diffusion rate constant (mg g^{-1} $min^{-0.5}$) and W is the Weber–Morris intercept (mg g^{-1}).

2.7.3. Error analysis

When fitting the specified models to the experimental data, care must be given to the selection of the regression method. The linearization of isotherm models in adsorption studies is a common error in data analysis [30,78–80]. Herein, all model parameters are calculated in R with the FME package by means of nonlinear regression with the Levenberg–Marquardt and pseudorandom-search algorithms in order to avoid propagated errors and inaccurate output results.

Furthermore, a combination of different statistical measures is advised to evaluate the models. The universal coefficient of determination R^2, for instance, is not only sensitive to extreme data points, but can also be easily manipulated by increasing the number of parameters in the model. Therefore, an additional statistical measure is used to complement the coefficient of determination. The coefficient of determination is given by:

$$R^2 = 1 - \frac{\sum_{i=1}^{n} \left(y_{i,exp} - y_{i,mod}\right)^2}{\sum_{i=1}^{n} \left(y_{i,exp} - \overline{y_{i,exp}}\right)^2} \tag{23}$$

where n is the number of data points, $y_{i,exp}$ is the experimental value of the independent variable, $y_{i,mod}$ is the modeled value of the independent variable and $\overline{y_{i,exp}}$ is the mean of the observed values of the independent variable.

The second statistical measure is Akaike's information criterion (AIC), which is particularly useful to compare models with different amounts of parameters. The criterion is given by [81]:

$$AIC = n\, ln\left(\frac{SSE}{n}\right) + 2n_p + \frac{2n_p\left(n_p + 1\right)}{n - \left(n_p + 1\right)} \tag{24}$$

Table 1
Summary of the properties[a] of the activated charcoal adsorbent.

S_{BET} ($m^2\ g^{-1}$)	S_{ext} ($m^2\ g^{-1}$)	S_{micro} ($m^2\ g^{-1}$)	V_{micro} ($cm^3\ g^{-1}$)	V_{tot} ($cm^3\ g^{-1}$)	W_{avg} (Å)
1209.28	646.83	562.45	0.27	0.77	64.50

[a] S_{BET}: specific surface area, S_{ext}: external surface area, S_{micro}: micropore surface area, V_{micro}: micropore volume, V_{tot}: total pore volume, W_{avg}: average pore width.

where SSE is the well-known sum of squares error and n_p is the number of parameters of the model. From Eq. (24), it can be derived that a small value of AIC corresponds to a good model fit. In addition, the evidence ratio Er can be used to compare two models:

$$Er = \frac{1}{e^{-0.5\Delta}} \tag{25}$$

where Δ is the absolute value of the difference in AIC values between the two models of comparison. It states the number of times one model is more supported by the experimental data than the other [30,82].

3. Results and discussions

3.1. Characterization of activated charcoal

A summary of the results from the characterization analysis of the porous texture of the adsorbent material is given in Table 1. The FTIR spectra of the adsorbent material before and after adsorption are presented in Fig. 1. As expected, the strongest signal of the activated charcoal is observed around 500 cm^{-1} which is indicative of C–C stretching [83]. The signals at 1060 and 1560 cm^{-1} are ascribed to stretching of C–O and C=C bonds, respectively. These might be caused by the activation process of the charcoal material [84–86]. More importantly, however, are the changes in the spectrum after adsorption of Solvent Red 135. The most prominent new signals are observed at 1730, 1380, 1200, 825, 760, and 725 cm^{-1}. All these signals are characteristic of the FTIR spectrum of Solvent Red 135 (Fig. 1), confirming the adherence of these dye molecules onto the adsorbent. The signals at 1730, 1380, and 1200 cm^{-1} are common for C=O stretching within cyclopentanone compounds, C-H bending, and C-N stretching in amines, respectively. The three signals at 825, 760 and 725 cm^{-1} are ascribed to C–Cl stretching of halo compounds [87]. All these chemical structures are represented in Solvent Red 135 (Fig. S1). From the SEM images, the morphology of the activated charcoal appears rough and irregular. After adsorption, the surface seems more smooth where pores and empty spaces are largely populated (Fig. 2). The latter indicates effective adsorption of the dye molecules.

3.2. Modeling and interpretation of adsorption isotherms

The experimental adsorption isotherms of Solvent Red 135 in o-xylene, limonene and butyl acetate are shown in Fig. 3. The adsorption capacity of the activated charcoal for the dye is largest in butyl acetate as acting solvent, while the lowest adsorption capacity is observed with o-xylene. This means that the dye experiences a relatively strong attraction towards o-xylene as opposed to butyl acetate. This can be explained by the interaction between aromatic π clouds, commonly referred to as π-π interactions. This phenomenon results in the aggregation of aromatic structures, a process known as π-stacking [88]. Hence, the benzene functional groups, present in both the dye and o-xylene molecules, induce an energetically important interaction. Since butyl acetate has no such aromatic π clouds available, its interaction with the dye is weaker. Moreover, as there are no free hydrogen atoms in the molecular structure of the dye (Fig. S1), there is no potential for hydrogen bonding, limiting the effect of solvent polarity. For limonene, the intermolecular attraction force is intermediate. This can be explained by the potential migration of π electrons from the propylene group towards the cyclohexene ring through the resonance effect, allowing for some preferential interaction with the dye molecules. In addition, and perhaps more importantly, the non-polar nature of limonene aligns better with the polarity of the dye compared to butyl acetate. The magnitude of intermolecular attraction forces between the solvents and the dye, is also indicated by the dye's solubility, with 1368 ± 79 mg L^{-1} in o-xylene, 88 ± 6 mg L^{-1} in limonene, and 61 ± 5 mg L^{-1} in butyl acetate. These solubilities were determined by gradually increasing the dye concentration at 293 K to the point where solid (precipitated) dye particles remained visibly undissolved for at least 24 h. With respect to the adsorption isotherms of PS, no observable adsorption took place in either of the three solvents (i.e. the change in absorbance for all samples is of the same magnitude as the standard deviation of the measurement). Furthermore, no significant differences in adsorption capacities for Solvent Red 135 were found for mixtures of the dye with 1.0 wt% PS (Fig. S3). The latter indicates that the competition for adsorption sites between the dye and polymer molecules is negligible under the specified conditions.

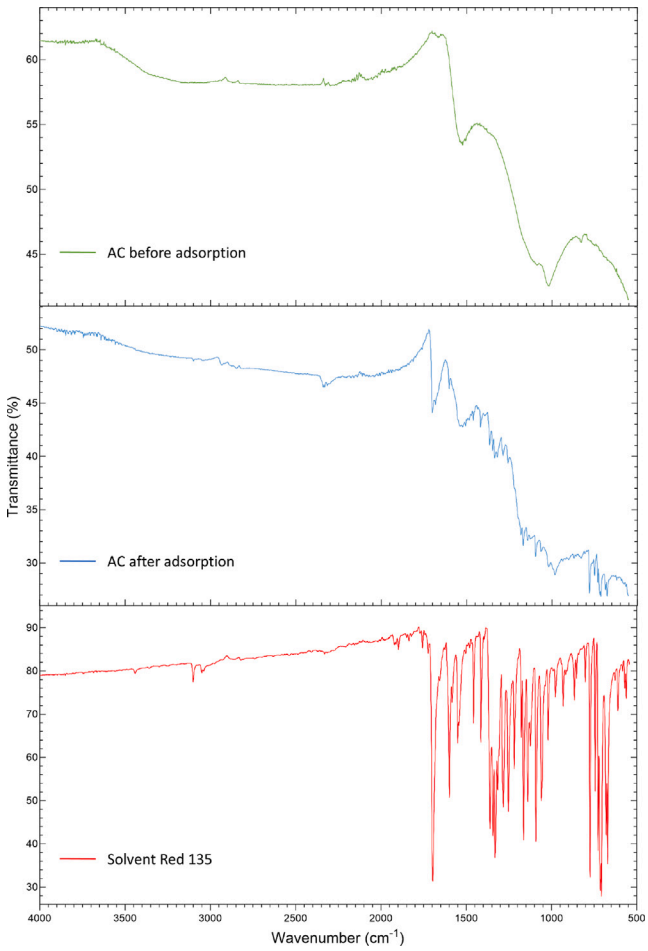

Fig. 1. FTIR spectra of activated charcoal (AC) before adsorption (top), after adsorption (middle), and of the dye Solvent Red 135 (bottom).

Table 2 provides a quantitative summary of the modeling results for the classical isotherm expressions. Among these, the Langmuir model performed best for all three solvents with R^2 ranging from 0.970 to 0.989 and AIC from 2.89 to 32.08. This suggests a monolayer coverage of the dye molecules with homogeneous distribution over the activated charcoal adsorbent surface, with little interaction between dye molecules [55]. Moreover, the separation factor $R_L = (1 + C_0 k_L)^{-1}$ proposed by the Langmuir theory, provides information about the type of isotherm [89]. Since R_L lies between 0 and 1 for all solutions, the

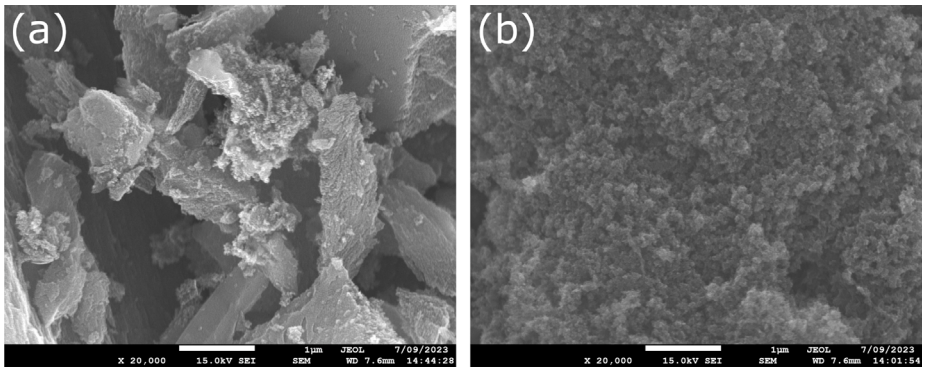

Fig. 2. SEM images of activated charcoal before (a) and after (b) adsorption of Solvent Red 135.

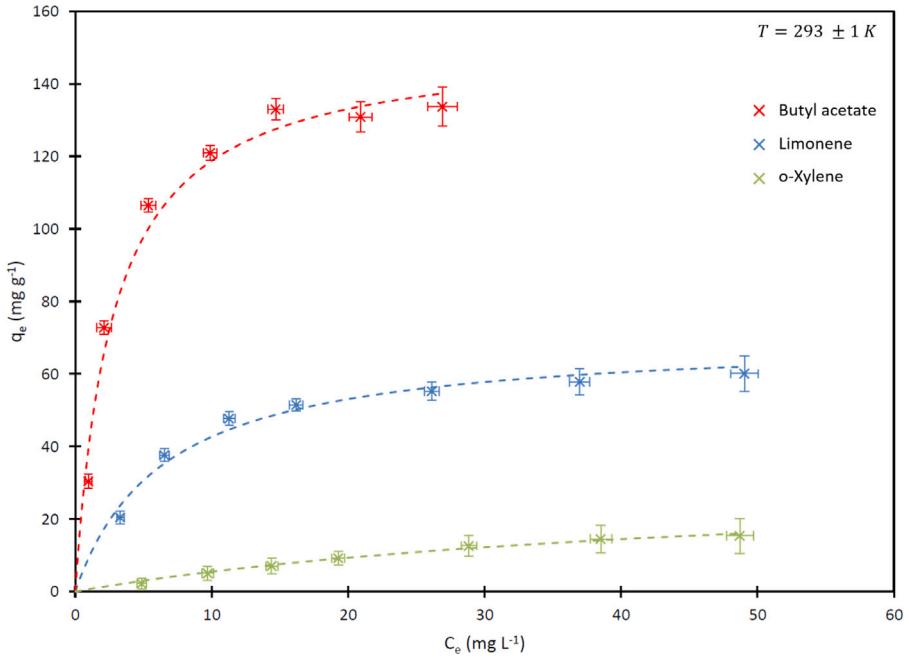

Fig. 3. Isotherms of Solvent Red 135 adsorption on activated charcoal in o-xylene (green crosses), limonene (blue crosses) and butyl acetate (red crosses) at 293 ± 1 K. Colored dashed lines represent the corresponding best fit according to the Langmuir isotherm model. Error bars represent the standard deviation of the corresponding variable.

adsorption is considered to be favorable. The corresponding maximum adsorption capacity for the dye q_{mL} is 31.91, 70.18 and 151.36 mg g^{-1} for o-xylene, limonene and butyl acetate as acting solvent, respectively (Fig. 3). Note that the R-P isotherm model presents identical R^2 values compared to the Langmuir model. However, the parameter b_R converged to 1 for all three solvents, meaning that the model in fact simplifies to the Langmuir expression. A similar observation can be made with respect to the BET expression, where the total number of adsorption layers n_B converged to 1. As a result, the model analogously simplifies to the Langmuir expression, explaining the identical R^2 values and the second BET model constant k_{B2} converging to its lower boundary. This, together with the relatively poor performance of the Freundlich expression, confirms the manifestation of homogeneous monolayer adsorption.

The modeling results of the statistical physics models are provided in Table 3. The monolayer expression describes the adsorption process most accurately for all three solvents, supporting the earlier findings of the classical modeling results. While the monolayer and multilayer expressions exhibit the same R^2 values, the N_2 parameter of the multilayer model converged to 0 in all cases, essentially suggesting monolayer adsorption. Therefore, the monolayer model is considered to reflect the adsorption mechanism in more detail. The steric parameter n is used to describe the geometry of the adsorbed dye molecules on the surface of the activated charcoal. If $n > 1$, the adsorbed species are assumed to be vertically oriented, while if $n < 1$ the adsorbed species are said to be horizontally oriented. Moreover, the adsorption mechanism is categorized as multi-molecular (i.e. one active site can hold multiple adsorbate molecules) if $n > 1$, or multi-docking (i.e. multiple functional groups of the adsorbent can hold one adsorbate molecule) when $n < 1$ [64,66,67,90–93]. Here, the steric parameters for the different solvents are very similar, namely 1.50, 1.51 and 1.48 for o-xylene, limonene and butyl acetate, respectively. Consequently, the solvent choice appears to have little impact on the adsorption mechanism of the dye. Since $n > 1$ for all three solvents (Table 3), it can be concluded that the dye adsorption was governed by a multi-molecular mechanism with predominantly vertically positioned dye molecules adsorbed to the surface of the activated charcoal. With respect to the density of occupied adsorption sites N_M, large differences were found between the solvents. The largest density was found for butyl acetate, suggesting a strong and directly proportional relation with the adsorption capacity, see Fig. 1. According to the monolayer statistical physics model, the adsorption capacity at saturation ($q_{sat} = nN_M$) was 20.05, 60.91 and 136.30 mg g^{-1} for the o-xylene, limonene and butyl acetate solvents, respectively. These adsorption capacities are

Table 2
Results of the classical isotherm modeling for Solvent Red 135 adsorption on activated charcoal in solutions of o-xylene, limonene and butyl acetate at 293 ± 1 K.

Model	Parameters	o-Xylene	Limonene	Butyl acetate
Langmuir	q_{mL} (mg g^{-1})	31.91	70.18	151.36
	k_L (L mg^{-1})	0.02	0.15	0.36
	$\boldsymbol{R^2}$	**0.989**	**0.970**	**0.972**
	$\boldsymbol{AIC}$	**2.89**	**18.37**	**32.08**
Freundlich	k_F (L mg^{-1})	1.11	18.94	51.33
	$\frac{1}{n}$	0.69	0.32	0.32
	$\boldsymbol{R^2}$	**0.970**	**0.852**	**0.839**
	$\boldsymbol{AIC}$	**3.85**	**29.47**	**44.31**
Temkin	b_T (J mol^{-1})	407.14	167.58	80.17
	k_T (L mg^{-1})	0.26	1.69	4.11
	$\boldsymbol{R^2}$	**0.982**	**0.928**	**0.928**
	$\boldsymbol{AIC}$	**4.53**	**24.46**	**38.63**
Dubinin–Radushkevich	q_{mD} (mg g^{-1})	12.90	57.08	127.00
	β (mol^2 kJ^{-2})	1.00E−05	2.84E−06	5.53E−07
	$\boldsymbol{R^2}$	**0.799**	**0.962**	**0.969**
	$\boldsymbol{AIC}$	**17.18**	**19.96**	**32.19**
Redlich–Peterson	k_R (L g^{-1})	0.66	10.88	55.20
	a_R (L mg^{-1})	0.02	0.15	0.36
	b_R	1.00	1.00	1.00
	$\boldsymbol{R^2}$	**0.989**	**0.970**	**0.972**
	$\boldsymbol{AIC}$	**4.11**	**25.37**	**39.08**
BET	n_B	1.00	1.00	1.00
	q_B (mg g^{-1})	31.91	70.14	151.32
	k_{B1} (L mg^{-1})	0.02	0.15	0.36
	k_{B2} (L mg^{-1})	1.00E−05	1.00E−05	1.00E−05
	$\boldsymbol{R^2}$	**0.989**	**0.970**	**0.972**
	$\boldsymbol{AIC}$	**18.11**	**39.37**	**53.08**

Table 3
Results of the statistical physics isotherm modeling for Solvent Red 135 adsorption on activated charcoal in solutions of o-xylene, limonene and butyl acetate at 293 ± 1 K.

Model	Parameters	o-Xylene	Limonene	Butyl acetate
Monolayer	n	1.50	1.51	1.48
	N_M (mg g^{-1})	13.37	40.22	92.24
	$C_{\frac{1}{2}}$ (mg L^{-1})	21.03	4.98	2.06
	$\boldsymbol{R^2}$	**0.998**	**0.996**	**0.994**
	$\boldsymbol{AIC}$	**7.53**	**11.14**	**28.97**
Double layer	n	1.13	1.20	1.67
	N_M (mg g^{-1})	8.85	25.57	40.43
	C_1 (mg L^{-1})	20.86	4.41	1.16
	C_2 (mg L^{-1})	21.99	5.05	2.05
	$\boldsymbol{R^2}$	**0.996**	**0.994**	**0.992**
	$\boldsymbol{AIC}$	**12.84**	**24.45**	**42.83**
Multilayer	n	1.50	1.51	1.48
	N_M (mg g^{-1})	13.37	40.22	92.24
	C_1 (mg L^{-1})	20.29	4.98	1.87
	C_2 (mg L^{-1})	24.19	19.45	13.38
	N_2	0.00	0.00	0.00
	$\boldsymbol{R^2}$	**0.998**	**0.996**	**0.994**
	$\boldsymbol{AIC}$	**48.47**	**67.14**	**84.97**

smaller than those suggested by the Langmuir expression (q_{mL}), yet are considered to be more accurate due to the more comprehensive approach of the statistical physics modeling.

Finally, the adsorption energy ΔE can be calculated based on the physicochemical parameters derived by the monolayer statistical physics model via [64,66,90–93]:

$$\Delta E = -RT\ ln\left(\frac{C_{\frac{1}{2}}}{C_S}\right) \tag{26}$$

where C_S represents the solubility of the dye in the corresponding solvent (mg L^{-1}). The values of the adsorption energies were 10.17, 7.00 and 8.25 kJ mol^{-1} for o-xylene, limonene and butyl acetate as solvent, respectively. This suggests that the adsorption of the dye on activated charcoal is endothermic for all three solvents. Furthermore, since all adsorption energy values are below 40 kJ mol^{-1}, the interactions between dye and adsorbent are physical in nature, indicating physisorption as opposed to chemisorption [64,91–93]. Future work should include different temperatures to investigate the thermodynamics in more detail.

Table 4
Results of the kinetic modeling for Solvent Red 135 adsorption at 40 mg L^{-1} on 10 mg of activated charcoal in 100 mL solutions of o-xylene, limonene and butyl acetate at 293 ± 1 K.

Model	Parameters	o-Xylene	Limonene	Butyl acetate
Pseudo-first-order	q_e (mg g^{-1})	26.41	65.02	122.98
	k_1 (min^{-1})	0.390	0.452	0.500
	$\boldsymbol{R^2}$	**0.839**	**0.960**	**0.976**
	$\boldsymbol{AIC}$	**26.99**	**32.46**	**44.19**
Pseudo-second-order	q_e (mg g^{-1})	26.41	65.02	122.98
	k_2 (g mg^{-1} min^{-1})	0.021	0.015	0.012
	$\boldsymbol{R^2}$	**0.933**	**0.991**	**0.995**
	$\boldsymbol{AIC}$	**15.58**	**12.84**	**25.08**
Elovich	a_E (mg g^{-1} min^{-1})	500.00	500.00	500.00
	b_E (g mg^{-1})	0.40	0.14	0.07
	$\boldsymbol{R^2}$	**0.915**	**0.806**	**0.671**
	$\boldsymbol{AIC}$	**18.91**	**53.19**	**81.14**
Weber–Morris	k_W (mg g^{-1} min$^{-0.5}$)	1.32	3.25	5.89
	W (mg g^{-1})	10.09	27.69	55.37
	$\boldsymbol{R^2}$	**0.404**	**0.252**	**0.187**
	$\boldsymbol{AIC}$	**48.63**	**75.53**	**92.70**

3.3. Analysis of adsorption kinetics

The adsorption kinetics of the red dye and the effect of solvent choice were investigated. Fig. 4 shows that adsorption equilibrium for all three solvents was reached after less than 120 min. Moreover, the superior adsorption capacity of activated charcoal with butyl acetate as acting solvent compared to limonene and o-xylene is confirmed. A summary of the kinetic modeling results is provided in Table 4. The performance of the pseudo-second-order model is dominant, combining the highest R^2 values with the lowest AIC for all three solvents. The rate constant k_2 is highest for o-xylene solutions, indicating a faster overall adsorption process. Considering the poor fit of the Weber–Morris model (R^2 from 0.187 to 0.404), it can be concluded that the adsorption rate is not solely controlled by intraparticle diffusion, but rather by a combination of internal and external mass transfer steps [72]. Similarly, due to the low R^2 values and the repeated convergence of the initial adsorption rate constant a_E to its boundary value, the Elovich model was deemed unfit to describe the adsorption process. Finally, no significant differences in adsorption kinetics were found for the mixtures of the dye with 1.0 wt% PS (Fig. S4).

3.4. Dye removal efficiency assessment

Fig. 5 illustrates the results of the removal efficiency study of Solvent Red 135. In general, the efficiency increases with the adsorbent dose as expected, due to the increase in available adsorption sites, and thus an increase in the total adsorbent surface area. The increase in removal efficiency, however, is the steepest at the beginning of the curves and flattens out when the maximum value of 100% is approached. For instance, the removal efficiency for butyl acetate solutions (without PS) increased with nearly 30% when the adsorbent dose was raised from 0.3 to 0.5 g L^{-1}, while an increase of merely 10% was observed when the adsorbent dose was further increased from 0.5 g L^{-1} to 1.0 g L^{-1} (Fig. 5). This can be explained by the decrease in concentration gradient of the adsorbate molecules between the solid and liquid phase as adsorption occurs, causing a reduction in driving force. In other words, the amount of unoccupied adsorption sites increases for higher adsorbent loadings. Similar adsorption behavior has been reported throughout literature for other liquid–solute systems [94–98].

Furthermore, the amount of dye molecules adsorbed for a particular adsorbent dose is significantly higher for butyl acetate as the acting solvent compared to limonene and o-xylene, especially for removal efficiencies greater than 50%. This is in agreement with the isotherm

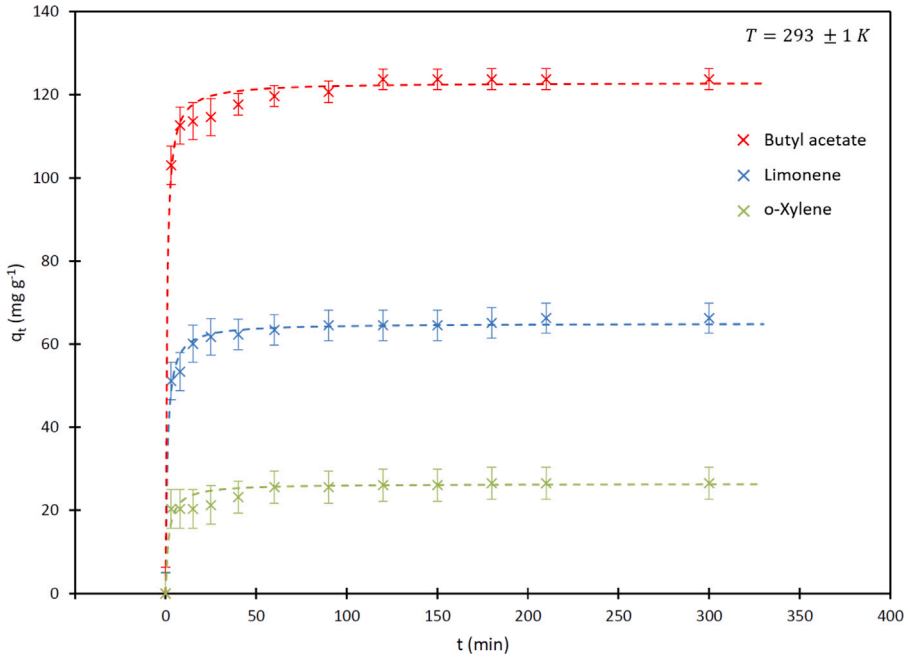

Fig. 4. Kinetics of Solvent Red 135 removal at 40 mg L^{-1} by 10 mg of activated charcoal in 100 mL solutions of xylene (green crosses), limonene (blue crosses) and butyl acetate (red crosses) at 293 ± 1 K. Colored dashed lines represent the corresponding best fit according to the pseudo-second-order kinetic model. Error bars represent the standard deviation.

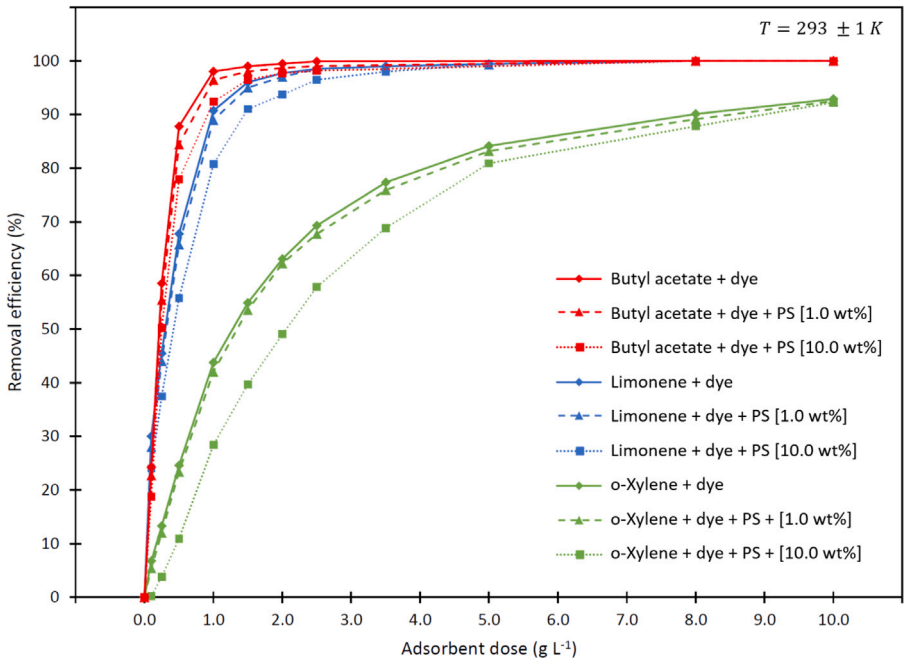

Fig. 5. Removal efficiency of Solvent Red 135 at 40 mg L^{-1} by activated charcoal in o-xylene (green), limonene (blue) and butyl acetate (red) at 293 ± 1 K as a function of adsorbent dose. Solutions of 100 mL with only dye (solid diamond lines), with a mixture of dye and 1.0 wt% PS (dashed triangle lines), and with a mixture of dye and 10.0 wt% PS (dotted square lines) are included.

results discussed in Section 3.2. For solutions without addition of PS, a removal efficiency of 99% was achieved at an adsorbent dose of approximately 1.5 and 3.5 g L^{-1} for butyl acetate and limonene as acting solvent, respectively. Corresponding solutions of o-xylene reached a removal efficiency of only 93% at the maximum adsorbent dose of 10 g L^{-1}. For mixtures of the dye with 1.0 wt% PS, no significant differences were found for the removal efficiencies up to roughly 50%. Minor deviations were observed for removal efficiencies higher than 50% (Fig. 5). Now, 99% removal efficiency was obtained for adsorbent doses of approximately 2.0 and 4.0 g L^{-1} for butyl acetate and limonene, respectively. These results suggest that there is little competitive adsorption between the dye and polymer molecules, which is supported by the findings in Section 3.2, revealing negligible adsorption of PS with respect to the experimental conditions.

Next, mixtures of the dye with 10.0 wt% PS were also investigated. For these viscous systems, statistically significant deviations are observed (t-test p-value < 0.05). In this case, the adsorbent dose that corresponds with 99% removal efficiency was approximately 3.3 g L^{-1} for butyl acetate, and 5.0 g L^{-1} for limonene as acting solvent. Despite the negligible adsorption of PS elaborated earlier, this might still be due to the slight competition of polymer and dye molecules for the available adsorption sites. As the initial concentration of PS is here approximately 2000 times higher than the one of the dye, adsorption of only a minor fraction of PS molecules may cause a significant reduction in the adsorption capacity towards the dye. The latter increases the required adsorbent dose to reach a certain level of dye removal. Another potential explanation revolves around the affinity between the polymer and dye molecules in the solvent system. Assuming non-ideal behavior, there might be significant attraction forces between the polymer and dye molecules, which in turn lowers the effective concentration of the dye. As a result, the dynamic adsorption equilibrium for the dye shifts towards the liquid phase, again lowering the adsorption capacity. Both phenomena might also occur simultaneously.

Finally, the reusability of the adsorbent for the removal of the dye in butyl acetate solutions was examined at an adsorbent dose of 0.5 g L^{-1}. The initial removal efficiency was 90%, where the one after the first, second and third regeneration cycle were 86, 81 and 79%, respectively (Fig. S5). This relative drop in removal efficiency is in agreement with literature and indicates that the activated charcoal can be regenerated with only minor adsorption capacity loss [52,53,99].

4. Conclusion

This study represents the initial assessment of adsorption as an effective technique for extracting additives in the context of plastic dissolution recycling. Activated charcoal has emerged as a promising adsorbent for removing a prevalent plastic dye from PS solutions. Three solvents were investigated: o-xylene as a traditional organic solvent, limonene as a green solvent, and butyl acetate as a more polar solvent. Adsorption experiments conducted at 293 K demonstrated that activated charcoal has the highest adsorption capacity for the dye in butyl acetate, while being negligible for PS in all three solvents. Removal efficiencies of 99% were achieved where a higher adsorbent dose was needed when the PS concentration was increased from 1 to 10 wt%. Through the use of classical and statistical physics modeling analyses, it was determined that the dye forms a monolayer on the activated charcoal and the adsorption process follows a multi-molecular mechanism, while the adsorption energy suggests an endothermic physisorption process. The results provide preliminary insights into the adsorption behavior of a common plastic additive on activated charcoal in a non-aqueous environment, offering potential applications in advanced plastics recycling. Further work on other additives and polymer types in combination with downstream processing (e.g. precipitation and degassing) is recommended to assess its full potential.

Declaration of competing interest

The authors declare that they have no known competing financial interests or personal relationships that could have appeared to influence the work reported in this paper.

Data availability

Data will be made available on request.

Acknowledgments

This work was performed in the framework of the Moonshot cluster SBO project PREFER (HBC.2020.2609 “The plastics refinery: no more waste”), with the financial support of VLAIO (Flemish Agency for Innovation and Entrepreneurship), Belgium via the Flemish spearhead cluster Catalisti. The graphical abstract was in part created with BioRender.com.

Appendix A. Supplementary data

Supplementary material related to this article can be found online at https://doi.org/10.1016/j.seppur.2023.125559.

References

[1] E. Baur, T.A. Osswald, N. Rudolph, in: E. Baur, T.A. Osswald, N. Rudolph (Eds.), Plastics Handbook, Hanser, 2019, pp. I–XXI, http://dx.doi.org/10.3139/9781569905609.fm, URL https://www.sciencedirect.com/science/article/pii/B978156990559350001X.

[2] Plastics Europe, Plastics—The Facts 2021 An analysis of European Plastics Production, Demand and Waste Data, Tech. rep., 2021, URL https://plasticseurope.org/knowledge-hub/plastics-the-facts-2021/.

[3] R. Geyer, J.R. Jambeck, K.L. Law, Production, use, and fate of all plastics ever made, Sci. Adv. 3 (7) (2017) 25–29, http://dx.doi.org/10.1126/sciadv.1700782.

[4] N. Evode, S.A. Qamar, M. Bilal, D. Barceló, H.M. Iqbal, Plastic waste and its management strategies for environmental sustainability, Case Stud. Chem. Environ. Eng. 4 (September) (2021) http://dx.doi.org/10.1016/j.cscee.2021.100142.

[5] H. Li, H.A. Aguirre-Villegas, R.D. Allen, X. Bai, C.H. Benson, G.T. Beckham, S.L. Bradshaw, J.L. Brown, R.C. Brown, V.S. Cecon, J.B. Curley, G.W. Curtzwiler, S. Dong, S. Gaddameedi, J.E. García, I. Hermans, M.S. Kim, J. Ma, L.O. Mark, M. Mavrikakis, O.O. Olafasakin, T.A. Osswald, K.G. Papanikolaou, H. Radhakrishnan, M.A. Sanchez Castillo, K.L. Sánchez-Rivera, K.N. Tumu, R.C. Van Lehn, K.L. Vorst, M.M. Wright, J. Wu, V.M. Zavala, P. Zhou, G.W. Huber, Expanding plastics recycling technologies: chemical aspects, technology status and challenges, Green Chem. 24 (23) (2022) 8899–9002, http://dx.doi.org/10.1039/d2gc02588d.

[6] G. Kwon, D.W. Cho, J. Park, A. Bhatnagar, H. Song, A review of plastic pollution and their treatment technology: A circular economy platform by thermochemical pathway, Chem. Eng. J. 464 (February) (2023) 142771, http://dx.doi.org/10.1016/j.cej.2023.142771.

[7] Ellen Macarthur Foundation, Plastics and the circular economy: Deep dive, 2022, URL https://ellenmacarthurfoundation.org/plastics-and-the-circular-economy-deep-dive.

[8] National Overview: Facts and Figures on Materials, Wastes and Recycling, United States Environmental Protection Agency, 2022, URL https://www.epa.gov/facts-and-figures-about-materials-waste-and-recycling/national-over-view-facts-and-figures-materials.

[9] K. Ragaert, L. Delva, K. Van Geem, Mechanical and chemical recycling of solid plastic waste, Waste Manag. 69 (2017) 24–58, http://dx.doi.org/10.1016/J.WASMAN.2017.07.044.

[10] D. Damayanti, D.R. Saputri, D.S.S. Marpaung, F. Yusupandi, A. Sanjaya, Y.M. Simbolon, W. Asmarani, M. Ulfa, H.S. Wu, Current prospects for plastic waste treatment, Polymers 14 (15) (2022) http://dx.doi.org/10.3390/polym14153133.

[11] M. Solis, S. Silveira, Technologies for chemical recycling of household plastics – A technical review and TRL assessment, Waste Manag. 105 (2020) 128–138, http://dx.doi.org/10.1016/J.WASMAN.2020.01.038.

[12] A. Eschenbacher, R.J. Varghese, M.S. Abbas-Abadi, K.M. Van Geem, Maximizing light olefins and aromatics as high value base chemicals via single step catalytic conversion of plastic waste, Chem. Eng. J. 428 (July 2021) (2022) 132087, http://dx.doi.org/10.1016/j.cej.2021.132087.

[13] P.R. Jadhao, E. Ahmad, K.K. Pant, K. D. P. Nigam, Advancements in the field of electronic waste Recycling: Critical assessment of chemical route for generation of energy and valuable products coupled with metal recovery, Sep. Purif. Technol. 289 (2022) 120773, http://dx.doi.org/10.1016/j.seppur.2022.120773, URL https://www.sciencedirect.com/science/article/pii/S1383586622003331.

[14] European Commission, Circular economy action plan, 2023, URL https://environment.ec.europa.eu/strategy/circular-economy-action-plan_en.

[15] M. Klotz, C. Oberschelp, C. Salah, L. Subal, S. Hellweg, The role of chemical and solvent-based recycling within a sustainable circular economy for plastics, Sci. Total Environ. 906 (1 January 2024) (2024) 167586, http://dx.doi.org/10.1016/j.scitotenv.2023.167586.

[16] S. Ügdüler, K.M. Van Geem, M. Roosen, E.I. Delbeke, S. De Meester, Challenges and opportunities of solvent-based additive extraction methods for plastic recycling, Waste Manag. 104 (2020) 148–182, http://dx.doi.org/10.1016/J.WASMAN.2020.01.003.

[17] A.M. Ferreira, I. Sucena, V. Otero, E.M. Angelin, M.J. Melo, J.A. Coutinho, Pretreatment of plastic waste: Removal of colorants from hdpe using biosolvents, Molecules 27 (1) (2022) http://dx.doi.org/10.3390/molecules27010098.

[18] H. Alojaly, K.Y. Benyounis, Packaging with plastics and polymeric materials, in: Encyclopedia of Materials: Plastics and Polymers, 2022, pp. 485–501, http://dx.doi.org/10.1016/b978-0-12-820352-1.00025-0.

[19] J.C.J. Bart, Additives in Polymers: Industrial Analysis and Applications, John Wiley & Sons, 2005.

[20] N. Neubauer, L. Scifo, J. Navratilova, A. Gondikas, A. Mackevica, D. Borschneck, P. Chaurand, V. Vidal, J. Rose, F. Von Der Kammer, W. Wohlleben, Nanoscale coloristic pigments: Upper limits on releases from pigmented plastic during environmental aging, in food contact, and by leaching, Environ. Sci. Technol. 51 (20) (2017) 11669–11680, http://dx.doi.org/10.1021/acs.est.7b02578.

[21] Recycling Plastics - The Creasolv® Process, Fraunhofer Institute for Process Engineering and Packaging IVV, URL https://www.ivv.fraunhofer.de/en/recycling-environment/recycling-plastics-creasolv.html.
[22] Unilever, Unilever develops new technology to tackle the global issue of plastic sachet waste, 2017, URL https://www.unilever.com/news/press-and-media/press-releases/2017/unilever-develops-new-technology-to-tackle-the-global-issue-of-plastic-sachet-waste/.
[23] APK AG, Newcycling® – the innovative recycling technology from APK AG, URL https://www.apk.group/en/.
[24] Cadel Recycling Lab, The deinking process, URL https://cadelrecyclinglab.com/en/.
[25] V. Komolprasert, A.R. Lawson, W.A. Hargraves, Analytical method for quantifying butyric acid, malathion, and diazinon in recycled poly(ethylene terephthalate), J. Agricult. Food Chem. 43 (8) (1995) 1963–1965, http://dx.doi.org/10.1021/jf00056a001.
[26] O. Moradi, G. Sharma, Emerging novel polymeric adsorbents for removing dyes from wastewater: A comprehensive review and comparison with other adsorbents, Environ. Res. 201 (2021) 111534, http://dx.doi.org/10.1016/J.ENVRES.2021.111534.
[27] B.S. Rathi, P.S. Kumar, Application of adsorption process for effective removal of emerging contaminants from water and wastewater, Environ. Pollut. 280 (2021) 116995, http://dx.doi.org/10.1016/j.envpol.2021.116995.
[28] A. Mudhoo, D. Mohan, C.U. Pittman, G. Sharma, M. Sillanpaa, Adsorbents for real-scale water remediation: Gaps and the road forward, J. Environ. Chem. Eng. 9 (4) (2021) http://dx.doi.org/10.1016/j.jece.2021.105380.
[29] N. Cheng, B. Wang, P. Wu, X. Lee, Y. Xing, M. Chen, B. Gao, Adsorption of emerging contaminants from water and wastewater by modified biochar: A review, Environ. Pollut. 273 (2021) 116448, http://dx.doi.org/10.1016/j.envpol.2021.116448.
[30] A. Bonilla-Petriciolet, D.I. Mendoza-Castillo, H.E. Reynel-Ávila, Adsorption processes for water treatment and purification, 2017, http://dx.doi.org/10.1007/978-3-319-58136-1.
[31] X. Pang, L. Sellaoui, D. Franco, M.S. Netto, J. Georgin, G. Luiz Dotto, M.K. Abu Shayeb, H. Belmabrouk, A. Bonilla-Petriciolet, Z. Li, Preparation and characterization of a novel mountain soursop seeds powder adsorbent and its application for the removal of crystal violet and methylene blue from aqueous solutions, Chem. Eng. J. 391 (November 2019) (2020) 123617, http://dx.doi.org/10.1016/j.cej.2019.123617.
[32] I. Salahshoori, M. Namayandeh Jorabchi, S. Ghasemi, M. Golriz, S. Wohlrab, H.A. Khonakdar, Advancements in wastewater Treatment: A computational analysis of adsorption characteristics of cationic dyes pollutants on amide Functionalized-MOF nanostructure MIL-53 (Al) surfaces, Sep. Purif. Technol. 319 (2023) 124081, http://dx.doi.org/10.1016/j.seppur.2023.124081, URL https://www.sciencedirect.com/science/article/pii/S1383586623009899.
[33] G. H. C. Prado, Y. Rao, A. de Klerk, Nitrogen removal from oil: A review, Energy Fuels 31 (1) (2016) 14–36, http://dx.doi.org/10.1021/acs.energyfuels.6b02779.
[34] D.S. Achilias, Chemical recycling of poly(methyl methacrylate) by pyrolysis. Potential use of the liquid fraction as a raw material for the reproduction of the polymer, Eur. Polym. J. 43 (6) (2007) 2564–2575, http://dx.doi.org/10.1016/j.eurpolymj.2007.02.044.
[35] G. Jiang, D. A. Sanchez Monsalve, P. Clough, Y. Jiang, G. A. Leeke, Understanding the dechlorination of chlorinated hydrocarbons in the pyrolysis of mixed plastics, ACS Sustain. Chem. Eng. 9 (4) (2021) 1576–1589, http://dx.doi.org/10.1021/acssuschemeng.0c06461.
[36] H. Niu, D. Zhao, G. Xie, Y. Yuan, W. Zhang, C. Zhang, C. Li, L. Cui, Deep dechlorination of model oil by reactive adsorption on porous oxides, Fuel 304 (2021) 121410, http://dx.doi.org/10.1016/J.FUEL.2021.121410.
[37] K. Drugkar, W. Rathod, T. Sharma, A. Sharma, J. Joshi, V.K. Pareek, L. Ledwani, U. Diwekar, Advanced separation strategies for up-gradation of bio-oil into value-added chemicals: A comprehensive review, Sep. Purif. Technol. 283 (2022) 120149, http://dx.doi.org/10.1016/j.seppur.2021.120149, URL https://www.sciencedirect.com/science/article/pii/S1383586621018542.
[38] P.J. Lu, H.C. Lin, W.T. Yu, J.M. Chern, Chemical regeneration of activated carbon used for dye adsorption, J. Taiwan Inst. Chem. Eng. 42 (2) (2011) 305–311, http://dx.doi.org/10.1016/j.jtice.2010.06.001.
[39] Y. Guo, E. Du, The effects of thermal regeneration conditions and inorganic compounds on the characteristics of activated carbon used in power plant, Energy Procedia 17 (2012) 444–449, http://dx.doi.org/10.1016/j.egypro.2012.02.118.
[40] K.Y. Foo, B.H. Hameed, A rapid regeneration of methylene blue dye-loaded activated carbons with microwave heating, J. Anal. Appl. Pyrolysis 98 (2012) 123–128, http://dx.doi.org/10.1016/j.jaap.2012.07.006.
[41] C.H. Weng, M.C. Hsu, Regeneration of granular activated carbon by an electrochemical process, Sep. Purif. Technol. 64 (2) (2008) 227–236, http://dx.doi.org/10.1016/j.seppur.2008.10.006.
[42] B. Bensebia, A. Dahmani, O. Bensebia, D. Barth, Analysis of the kinetics of regeneration of bidispersed activated granular carbon, by supercritical carbon dioxide, J. Supercrit. Fluids 54 (2) (2010) 178–189, http://dx.doi.org/10.1016/j.supflu.2010.04.005.
[43] M. El Gamal, H.A. Mousa, M.H. El-Naas, R. Zacharia, S. Judd, Bio-regeneration of activated carbon: A comprehensive review, Sep. Purif. Technol. 197 (January) (2018) 345–359, http://dx.doi.org/10.1016/j.seppur.2018.01.015.
[44] ChemicalBook, Solvent red 135, 2022, URL https://www.chemicalbook.com/ProductChemicalPropertiesCB6434782_EN.htm.
[45] A.H. Tullo, Plastic has a problem; is chemical recycling the solution?, 2019, URL https://cen.acs.org/environment/recycling/Plastic-problem-chemical-recycling-solution/97/i39.
[46] S. Chemat, V. Tomao, F. Chemat, Limonene as green solvent for extraction of natural products, in: A. Mohammad (Ed.), Green Solvents I: Properties and Applications in Chemistry, Springer Netherlands, Dordrecht, 2012, pp. 175–186, http://dx.doi.org/10.1007/978-94-007-1712-1_5.
[47] O. Amrhar, L. El Gana, M. Mobarak, Calculation of adsorption isotherms by statistical physics models: a review, Environ. Chem. Lett. 19 (6) (2021) 4519–4547, http://dx.doi.org/10.1007/s10311-021-01279-8.
[48] S. Brunauer, P.H. Emmett, E. Teller, Adsorption of gases in multimolecular layers, J. Am. Chem. Soc. 60 (2) (1938) 309–319, http://dx.doi.org/10.1021/ja01269a023.
[49] B.C. Lippens, B.G. Linsen, J. Boer, Studies on pore systems in catalysts I. The adsorption of nitrogen; apparatus and calculation, J. Catal. 3 (1) (1964) 32–37, http://dx.doi.org/10.1016/0021-9517(64)90089-2, URL https://www.sciencedirect.com/science/article/pii/0021951764900892.
[50] E.P. Barrett, L.G. Joyner, P.P. Halenda, The determination of pore volume and area distributions in porous substances. I. Computations from nitrogen isotherms, J. Am. Chem. Soc. 73 (1) (1951) 373–380, http://dx.doi.org/10.1021/ja01145a126.
[51] E. Hansen, N.H. Nilsson, D. Lithner, C. Lassen, Hazardous substances in plastic materials, 2013, p. 148, URL http://www.miljodirektoratet.no/no/Publikasjoner/Publikasjoner/2013/Februar/Hazardous_substances_in_plastic_materials/.
[52] E.H. Ezechi, S.R.B.M. Kutty, A. Malakahmad, M.H. Isa, Characterization and optimization of effluent dye removal using a new low cost adsorbent: Equilibrium, kinetics and thermodynamic study, Process Saf. Environ. Prot. 98 (2015) 16–32, http://dx.doi.org/10.1016/J.PSEP.2015.06.006.
[53] M. Naushad, A.A. Alqadami, Z.A. AlOthman, I.H. Alsohaimi, M.S. Algamdi, A.M. Aldawsari, Adsorption kinetics, isotherm and reusability studies for the removal of cationic dye from aqueous medium using arginine modified activated carbon, J. Mol. Liq. 293 (2019) 111442, http://dx.doi.org/10.1016/j.molliq.2019.111442.
[54] I. Langmuir, The adsorption of gases on plane surfaces of glass, mica and platinum, J. Am. Chem. Soc. 40 (9) (1918) 1361–1403, http://dx.doi.org/10.1021/ja02242a004.
[55] P. Atkins, P. Julio, Atkin's Physical Chemistry, Oxford University Press, New York, 2006.
[56] H. Freundlich, Über die adsorption in lösungen, Z. Phys. Chem. 57U (1) (1907) 385–470, http://dx.doi.org/10.1515/zpch-1907-5723.
[57] M.I. Temkin, Kinetics of ammonia synthesis on promoted iron catalysts, Acta Phys. Chem. 12 (1940) 327–356.
[58] N.D. Hutson, R.T. Yang, Theoretical basis for the Dubinin-Radushkevitch (D-R) adsorption isotherm equation, Adsorption 3 (3) (1997) 189–195, http://dx.doi.org/10.1007/BF01650130, URL https://www.scopus.com/inward/record.uri?eid=2-s2.0-0030646131&doi=10.1007%2FBF01650130&partnerID=40&md5=df00ddfcd1ac18ec13a6d87ff20c1797.
[59] O. Redlich, D.L. Peterson, A useful adsorption isotherm, J. Phys. Chem. 63 (6) (1959) 1024, http://dx.doi.org/10.1021/j150576a611.
[60] R. Sips, On the structure of a catalyst surface, J. Chem. Phys. 16 (5) (1948) 490–495, http://dx.doi.org/10.1063/1.1746922.
[61] W. Fritz, E.-U. Schluender, Simultaneous adsorption equilibria of organic solutes in dilute aqueous solutions on activated carbon, Chem. Eng. Sci. 29 (5) (1974) 1279–1282, http://dx.doi.org/10.1016/0009-2509(74)80128-4, URL https://www.sciencedirect.com/science/article/pii/0009250974801284.
[62] A. Ebadi, J.S.S. Mohammadzadeh, A.T. Khudiev, What is the correct form of BET isotherm for modeling liquid phase adsorption? Adsorption 15 (2009) 65–73.
[63] X. Pang, L. Sellaoui, D. Franco, G.L. Dotto, J. Georgin, A. Bajahzar, H. Belmabrouk, A. Ben Lamine, A. Bonilla-Petriciolet, Z. Li, Adsorption of crystal violet on biomasses from pecan nutshell, para chestnut husk, araucaria bark and palm cactus: Experimental study and theoretical modeling via monolayer and double layer statistical physics models, Chem. Eng. J. 378 (June) (2019) http://dx.doi.org/10.1016/j.cej.2019.122101.
[64] A.S. Abu Sharib, A. Bonilla-Petriciolet, A.Q. Selim, E.A. Mohamed, M.K. Seliem, Utilizing modified weathered basalt as a novel approach in the preparation of Fe3O4 nanoparticles: Experimental and theoretical studies for crystal violet adsorption, J. Environ. Chem. Eng. 9 (6) (2021) http://dx.doi.org/10.1016/j.jece.2021.106220.
[65] H. Wang, Z. Li, S. Yahyaoui, H. Hanafy, M.K. Seliem, A. Bonilla-Petriciolet, G. Luiz Dotto, L. Sellaoui, Q. Li, Effective adsorption of dyes on an activated carbon prepared from carboxymethyl cellulose: Experiments, characterization and advanced modelling, Chem. Eng. J. 417 (October 2020) (2021) 128116, http://dx.doi.org/10.1016/j.cej.2020.128116.
[66] H. Xue, X. Gao, M.K. Seliem, M. Mobarak, R. Dong, X. Wang, K. Fu, Q. Li, Z. Li, Efficient adsorption of anionic azo dyes on porous heterostructured MXene/biomass activated carbon composites: Experiments, characterization, and theoretical analysis via advanced statistical physics models, Chem. Eng. J. 451 (2023) 138735, http://dx.doi.org/10.1016/J.CEJ.2022.138735.

[67] Z. Li, L. Sellaoui, G. Luiz Dotto, A. Bonilla-Petriciolet, A. Ben Lamine, Understanding the adsorption mechanism of phenol and 2-nitrophenol on a biopolymer-based biochar in single and binary systems via advanced modeling analysis, Chem. Eng. J. 371 (March) (2019) 1–6, http://dx.doi.org/10.1016/j.cej.2019.04.035.

[68] Z. Li, L. Sellaoui, D. Franco, M.S. Netto, J. Georgin, G.L. Dotto, A. Bajahzar, H. Belmabrouk, A. Bonilla-Petriciolet, Q. Li, Adsorption of hazardous dyes on functionalized multiwalled carbon nanotubes in single and binary systems: Experimental study and physicochemical interpretation of the adsorption mechanism, Chem. Eng. J. 389 (January) (2020) http://dx.doi.org/10.1016/j.cej.2020.124467.

[69] X.-L. Gong, H.-Q. Lu, K. Li, W. Li, Effective adsorption of crystal violet dye on sugarcane bagasse–bentonite/sodium alginate composite aerogel: Characterisation, experiments, and advanced modelling, Sep. Purif. Technol. 286 (2022) 120478, http://dx.doi.org/10.1016/j.seppur.2022.120478, URL https://www.sciencedirect.com/science/article/pii/S1383586622000387.

[70] X. Wang, Q. Xu, L. Zhang, L. Pei, H. Xue, Z. Li, Adsorption of methylene blue and congo red from aqueous solution on 3D MXene/carbon foam hybrid aerogels: A study by experimental and statistical physics modeling, J. Environ. Chem. Eng. 11 (1) (2023) http://dx.doi.org/10.1016/j.jece.2022.109206.

[71] H. Qiu, L. Lv, B.C. Pan, Q.J. Zhang, W.M. Zhang, Q.X. Zhang, Critical review in adsorption kinetic models, J. Zhejiang Univ.: Sci. A 10 (5) (2009) 716–724, http://dx.doi.org/10.1631/jzus.A0820524.

[72] J. Wang, X. Guo, Adsorption kinetic models: Physical meanings, applications, and solving methods, J. Hazard. Mater. 390 (2020) 122156, http://dx.doi.org/10.1016/J.JHAZMAT.2020.122156.

[73] Q. Tan, X. Jia, R. Dai, H. Chang, M.W. Woo, H. Chen, Synthesis of a novel magnetically recyclable starch-based adsorbent for efficient adsorption of crystal violet dye, Sep. Purif. Technol. 320 (2023) 124157, http://dx.doi.org/10.1016/j.seppur.2023.124157, URL https://www.sciencedirect.com/science/article/pii/S1383586623010651.

[74] S. Lagergren, About the theory of so-called adsorption of soluble substances, in: Sven. Vetenskapsakad. Handingarl, Vol. 24, 1898, pp. 1–39, URL https://cir.nii.ac.jp/crid/1570009750361875328.

[75] Y.S. Ho, D.A.J. Wase, C.F. Forster, Removal of lead ions from aqueous solution using sphagnum moss peat as absorbent, Water SA 22 (3) (1996) 219–224, URL https://www.scopus.com/inward/record.uri?eid=2-s2.0-0029809629&partnerID=40&md5=213c089a6bdcc6b10d9035edf41d9ae5.

[76] S.Y. Elovich, O.G. Larinov, Theory of adsorption from solutions of non electrolytes on solid (I) equation adsorption from solutions and the analysis of its simplest form, (II) verification of the equation of adsorption isotherm from solutions, Izv. Akad. Nauk. SSSR, Otd. Khim. Nauk 2 (2) (1962) 209–216, URL https://www.scopus.com/inward/record.uri?eid=2-s2.0-2542639994&partnerID=40&md5=684023d93229c240d0bce3b3b3659d1c.

[77] W.J. Weber, J.C. Morris, Kinetics of adsorption on carbon from solution, ASCE Sanit. Eng. Div. J. 1 (2) (1963) 1–2, URL https://www.scopus.com/inward/record.uri?eid=2-s2.0-84981279868&partnerID=40&md5=1413e05f570c5f71612379d9a47ac010.

[78] M.I. El-Khaiary, G.F. Malash, Common data analysis errors in batch adsorption studies, Hydrometallurgy 105 (3–4) (2011) 314–320, http://dx.doi.org/10.1016/j.hydromet.2010.11.005.

[79] K.Y. Foo, B.H. Hameed, Insights into the modeling of adsorption isotherm systems, Chem. Eng. J. 156 (1) (2010) 2–10, http://dx.doi.org/10.1016/j.cej.2009.09.013.

[80] J.P. Simonin, On the comparison of pseudo-first order and pseudo-second order rate laws in the modeling of adsorption kinetics, Chem. Eng. J. 300 (2016) 254–263, http://dx.doi.org/10.1016/j.cej.2016.04.079.

[81] H. Akaike, Information theory and an extension of the maximum likelihood principle, in: E. Parzen, K. Tanabe, G. Kitagawa (Eds.), Selected Papers of Hirotugu Akaike, Springer New York, New York, NY, 1998, pp. 199–213, http://dx.doi.org/10.1007/978-1-4612-1694-0_15.

[82] D.R. Anderson, K.P. Burnham, Avoiding pitfalls when using information-theoretic methods, J. Wildl. Manage. 66 (3) (2002) 912–918, URL http://www.jstor.org/stable/3803155.

[83] A.I. Bakti, P.L. Gareso, Characterization of active carbon prepared from coconuts shells using FTIR, XRD and SEM techniques, J. Ilmiah Pendidikan Fisika Al-Biruni 7 (1) (2018) 33–39, http://dx.doi.org/10.24042/jipfalbiruni.v7i1.2459.

[84] R. Ali, Z. Aslam, R.A. Shawabkeh, A. Asghar, I.A. Hussein, BET, FTIR, and RAMAN characterizations of activated carbon from waste oil fly ash, Turk. J. Chem. 44 (2) (2020) 279–295, http://dx.doi.org/10.3906/KIM-1909-20.

[85] S. Shin, J. Jang, S.H. Yoon, I. Mochida, A study on the effect of heat treatment on functional groups of pitch based activated carbon fiber using FTIR, Carbon 35 (12) (1997) 1739–1743, http://dx.doi.org/10.1016/S0008-6223(97)00132-2.

[86] Y. Ji, T. Li, L. Zhu, X. Wang, Q. Lin, Preparation of activated carbons by microwave heating KOH activation, Appl. Surf. Sci. 254 (2) (2007) 506–512, http://dx.doi.org/10.1016/j.apsusc.2007.06.034.

[87] Merck KGaA, IR spectrum table & chart, URL https://www.sigmaaldrich.com/BE/en/technical-documents/technical-article/analytical-chemistry/photometry-and-reflectometry/ir-spectrum-table.

[88] C.R. Martinez, B.L. Iverson, Rethinking the term "pi-stacking", Chem. Sci. 3 (7) (2012) 2191–2201, http://dx.doi.org/10.1039/c2sc20045g.

[89] T.W. Weber, R.K. Chakravorti, Pore and solid diffusion models for fixed-bed adsorbers, AIChE J. 20 (2) (1974) 228–238, http://dx.doi.org/10.1002/aic.690200204.

[90] Z. Li, L. Sellaoui, G.L. Dotto, A.B. Lamine, A. Bonilla-Petriciolet, H. Hanafy, H. Belmabrouk, M.S. Netto, A. Erto, Interpretation of the adsorption mechanism of Reactive Black 5 and Ponceau 4R dyes on chitosan/polyamide nanofibers via advanced statistical physics model, J. Mol. Liq. 285 (2019) 165–170, http://dx.doi.org/10.1016/j.molliq.2019.04.091.

[91] E.A. Mohamed, A.Q. Selim, S.A. Ahmed, L. Sellaoui, A. Bonilla-Petriciolet, A. Erto, Z. Li, Y. Li, M.K. Seliem, H2O2-activated anthracite impregnated with chitosan as a novel composite for cr(VI) and methyl orange adsorption in single-compound and binary systems: Modeling and mechanism interpretation, Chem. Eng. J. 380 (July 2019) (2020) 122445, http://dx.doi.org/10.1016/j.cej.2019.122445.

[92] H.S. Ramadan, M. Mobarak, E.C. Lima, A. Bonilla-Petriciolet, Z. Li, M.K. Seliem, Cr(VI) adsorption onto a new composite prepared from Meidum black clay and pomegranate peel extract: Experiments and physicochemical interpretations, J. Environ. Chem. Eng. 9 (4) (2021) http://dx.doi.org/10.1016/j.jece.2021.105352.

[93] L. Sellaoui, A. Gómez-Avilés, F. Dhaouadi, J. Bedia, A. Bonilla-Petriciolet, S. Rtimi, C. Belver, Adsorption of emerging pollutants on lignin-based activated carbon: Analysis of adsorption mechanism via characterization, kinetics and equilibrium studies, Chem. Eng. J. 452 (2023) 139399, http://dx.doi.org/10.1016/J.CEJ.2022.139399.

[94] A. Essekri, A. Hsini, Y. Naciri, M. Laabd, Z. Ajmal, M. El Ouardi, A. Ait Addi, A. Albourine, Novel citric acid-functionalized brown algae with a high removal efficiency of crystal violet dye from colored wastewaters: insights into equilibrium, adsorption mechanism, and reusability, Int. J. Phytoremediation 23 (4) (2021) 336–346, http://dx.doi.org/10.1080/15226514.2020.1813686.

[95] A.R. Kaveeshwar, S.K. Ponnusamy, E.D. Revellame, D.D. Gang, M.E. Zappi, R. Subramaniam, Pecan shell based activated carbon for removal of iron(II) from fracking wastewater: Adsorption kinetics, isotherm and thermodynamic studies, Process Saf. Environ. Prot. 114 (2018) 107–122, http://dx.doi.org/10.1016/j.psep.2017.12.007.

[96] M. Laabd, H. Chafai, A. Essekri, M. Elamine, S.A. Al-Muhtaseb, R. Lakhmiri, A. Albourine, Single and multi-component adsorption of aromatic acids using an eco-friendly polyaniline-based biocomposite, Sustain. Mater. Technol. 12 (March) (2017) 35–43, http://dx.doi.org/10.1016/j.susmat.2017.04.004.

[97] T.P.M. Chu, N.T. Nguyen, T.L. Vu, T.H. Dao, L.C. Dinh, H.L. Nguyen, T.H. Hoang, T.S. Le, T.D. Pham, Synthesis, characterization, and modification of alumina nanoparticles for cationic dye removal, Materials 12 (3) (2019) 1–15, http://dx.doi.org/10.3390/ma12030450.

[98] D. Wu, Y. Wang, Y. Li, Q. Wei, L. Hu, T. Yan, R. Feng, L. Yan, B. Du, Phosphorylated chitosan/CoFe2O4 composite for the efficient removal of Pb(II) and Cd(II) from aqueous solution: Adsorption performance and mechanism studies, J. Mol. Liq. 277 (2019) 181–188, http://dx.doi.org/10.1016/j.molliq.2018.12.098.

[99] R. Ganjoo, S. Sharma, A. Kumar, M.M.A. Daouda, Activated carbon: Fundamentals, classification, and properties, in: Activated Carbon: Progress and Applications, The Royal Society of Chemistry, 2023, http://dx.doi.org/10.1039/BK9781839169861-00001.